A temptative to reach a visual singular configuration using Halley's method.

Mohammed Marey and François Chaumette

Abstract—Image-based visual servoing has been found to give satisfactory accurate and robust results. However, singularity and local minima may appear causing stability and convergence problems. In this paper, we present new control schemes based on Halley's method as a temptative to obtain a robust system even when the desired configuration is singular. The new control scheme use the first and the second order derivatives of the error to be regulated to zero. Hessian matrices of an image point are thus determined to be used in the control schemes. Preliminary experimental results obtained on a 6 dof eye-in-hand system shows that a more accurate positioning can be obtained compared with classical methods.

I. INTRODUCTION

As pointed out in [2], convergence and stability problems may occur in some cases in image-based visual servoing. This happens when the system reaches a local minimum or when it crosses or reaches a singular configuration. Such singular configurations correspond to a loss of rank of the Jacobian matrix that relates the features used as input of the control scheme to the control parameters. That Jacobian matrix is named the interaction matrix [15], [3] when the control parameters are the six components of the instantaneous sensor velocity $\mathbf{v}$ (to recall that the considered working space is the Special Euclidean group SE_3 in which Lie algebra properties can be applied).

Several singular configurations in image-based visual servoing have been exhibited in the litterature. The most well known one appears for a target composed of three points. Indeed, for that target, when the camera optical axis lies on the surface of a cylinder built from these three points, the interaction matrix related to the Cartesian coordinates of the three image points is singular (with rank 5) [11], while it is of full rank 6 as soon as the camera optical axis lies outside of this surface. The same singular configurations exist whatever the image features selected to represent the three points (cylindrical coordinates of the points, parameters representing the three straight lines that can be defined from the three points, etc.) Another singular configuration has been exhibited in [1]: if the target is a circle, then the interaction matrix related to any set of parameters that represents the image of that circle, which is an ellipse, is always of rank 5, but when the circle appears in the image as a centered circle, in which case the interaction matrix if of rank 3. More general singular configurations can be exhibited: whatever the set $\mathbf{s}$ of features selected and its desired value $\mathbf{s}^*$, the interaction matrix related to $\|\mathbf{s} - \mathbf{s}^*\|$ is always of full rank 1 but when $\mathbf{s} = \mathbf{s}^*$, in which case the interaction matrix is null [6]. This case is extremely problematic since the singularity occurs at the desired configuration where we would like the system to be stable and robust, while it is well known that classical control schemes are unstable and very sensitive to noise and perturbations around singular configurations.

Usually, these singular configurations are avoided trivially by selecting features such that their interaction matrix is always of full rank, that is by considering a fourth point when the original target is a set of three points, or by considering two circles or a circle and a point instead of just a circle, or by using $\mathbf{s}$ instead of $\|\mathbf{s} - \mathbf{s}^*\|$. This is not completely satisfactory from a scientific point of view, and may not be always possible in practice, when only three points can be extracted in the image for instance.

When the redundancy framework can be applied, that is when the main task does not control all the robot degrees of freedom (dof), a secondary objective can be designed to try avoid the singular configurations [13], [9]. Once again, this method can not always be used, typically when the task constrains all the robot dof. Furthermore, it is not efficient if the goal is to reach a singular configuration. To deal with this problem, a classical solution in robotics is to use the damped-least-squares inverse [16], [12], [5], [4] instead of the Moore-Penrose pseudo inverse. This method, which artificially increases the lowest singular values of the Jacobian matrix, reduces the effect of the singularity in terms of robustness, but decreases the precision of the control. Finally, a regularization technique has recently been introduced in [6]. It also allows reducing the effect of the singularity, but with the price of decreasing the convergence speed, which is inefficient if the task consists in tracking a moving target.

In this paper, we propose new control schemes to try to reach a singular configuration. It is based on Halley's method, which uses a second order minimization step. After analysing in Section II the behavior of the classical control schemes in a singular configuration, we present the new control schemes in Section III. Theu are based on the Hessian matrices of the selected features. We thus determine in Section IV the Hessian matrices of the Cartesian coordinates of an image point. Finally, experimental results are presented in Section V.

Mohammed Marey and François Chaumette are with INRIA, Centre Rennes-Bretagne Atlantique, IRISA, Campus de Beaulieu, F35042 Rennes-cedex, France. E-mail: `Firstname.Name@irisa.fr`

II. ANALYSIS OF CLASSICAL CONTROL SCHEMES

Let $\mathbf{s} \in \mathbb{R}^k$ be the vector of the selected k visual features, $\mathbf{s}^*$ their desired value and $\mathbf{v} \in \mathbb{R}^6$ the instantaneous velocity of the camera. Most classical control laws have the following form:

$$\mathbf{v} = -\lambda \, \widehat{\mathbf{L_s}}^+ (\mathbf{s} - \mathbf{s}^*) \qquad (1)$$

where λ is a gain and $\widehat{\mathbf{L_s}}^+$ is the pseudoinverse of an estimation or an approximation of the interaction matrix related to $\mathbf{s}$ (defined such that $\dot{\mathbf{s}} = \mathbf{L_s} \mathbf{v}$ where $\mathbf{v} = (v, \omega)$ with v the translational velocity and ω the rotational one). Different forms for $\widehat{\mathbf{L_s}}$ have been proposed in the past [3]. For simplicity, we consider that all values can be computed accurately, leading to the following choices

$$1): \widehat{\mathbf{L_s}} = \mathbf{L_{s^*}} \qquad (2)$$
$$2): \widehat{\mathbf{L_s}} = \mathbf{L_{s(t)}} \qquad (3)$$
$$3): \widehat{\mathbf{L_s}} = (\mathbf{L_{s^*}} + \mathbf{L_{s(t)}})/2. \qquad (4)$$

In the first case, $\widehat{\mathbf{L_s}}$ is constant during all the servo since it is the value of the interaction matrix computed at the desired configuration. In the second case, $\widehat{\mathbf{L_s}}$ changes at each iteration of the servo since the current value of the interaction matrix is used. Finally, in the third case, the mean of these two values is used [8]. These three usual choices for $\widehat{\mathbf{L_s}}$ when used with (1) define three distinct control laws, that we denote D, C and M (for desired, current, and mean respectively).

In this paper, we are interested in the case where the interaction matrix is singular at the desired configuration, that is when $\mathbf{L_{s^*}}$ is singular. In that case, control law D is of course inefficient since it is subject to numerous local minima. Indeed, all configurations such that:

$$(\mathbf{s} - \mathbf{s}^*) \in \mathcal{N}\left(\mathbf{L_{s^*}^+}\right)$$

(where $\mathcal{N}(\mathbf{A})$ is the null space of matrix $\mathbf{A}$) correspond to a local minimum, and such configurations are generally numerous since $\mathcal{N}(\mathbf{L_{s^*}^+})$ is at least of dimension 1. If the initial error $\mathbf{s}_i - \mathbf{s}^*$ is large and $\mathbf{L_{s_i}}$ is not singular, control law C can be used at the beginning of the servo, but, as soon as $\mathbf{s} - \mathbf{s}^*$ will become small, the system will be unstable since it nears the singularity. The same comment can unfortunately be done for control law M, even if we could hope for some smoothing effects of the singularity thanks to the use of the constant matrix $\mathbf{L_{s^*}}$ in M. This simple analysis of the behavior of control laws D, C, and M will be confirmed in Section V through experimental results.

To avoid the unstability near the singularity of all control schemes based on the interaction matrix only, we could think of using second order schemes, such as the one based on the classical Newton minimization method. It is given by (see [8] for instance):

$$\mathbf{v} = -\lambda \, \mathbf{K}_1^+ \mathbf{L_s^\top} (\mathbf{s} - \mathbf{s}^*) \qquad (5)$$

where

$$\mathbf{K}_1 = \mathbf{L_s^\top} \mathbf{L_s} + \sum_{i=1}^{k} \mathbf{H}_{s_i}(s_i - s_i^*)$$

$\mathbf{H}_{s_i}$ being the Hessian matrix of the i-th component of $\mathbf{s}$. Unfortunately, the convergence domain of this control scheme is generally very limited due to the fact that the Hessian is not always positive definite (see Section IV-B). Furthermore, all configurations such that $\mathbf{L_s}$ is singular and

$$(\mathbf{s} - \mathbf{s}^*) \in \mathcal{N}\left(\mathbf{L_s^\top}\right)$$

correspond to a local minimum since we have in that case $\mathbf{v} = \mathbf{L_s^\top}(\mathbf{s} - \mathbf{s}^*) = 0$. This is also of course the same for the basic control scheme

$$\mathbf{v} = -\lambda \, \mathbf{L_s^\top}(\mathbf{s} - \mathbf{s}^*)$$

based on the steepest descent and usually named gradient method.

All control schemes described above being not satisfactory when trying to reach a singular configuration, we propose new control schemes, based on Halley's method, in the next section.

III. HALLEY'S METHOD

A. Scalar case

Halley's method is well known in the numerical analysis community to find a root of a function $f(x)$ (that is to find x_r such that $f(x_r) = 0$) [14]. As classical gradient and Newton methods, it is an iterative algorithm that can be applied if function f is continuous and twice differentiable. It is based on the second order Taylor expansion of f:

$$f(x) = f(x_n) + f'(x_n)(x - x_n) + \frac{1}{2} \, f''(x_n)(x - x_n)^2 \quad (6)$$

where x_n is the estimate of x_r at iteration n of the algorithm. Let x_{n+1} be the root of (6). It can be written:

$$x_{n+1} = x_n - \frac{f(x_n)}{2f'(x_n) - \frac{1}{2}f''(x_n)(x_{n+1} - x_n)}$$

This equation can not be used directly since x_{n+1} appears both in its left and right sides. However, using on the right side, the result of the Newton-Raphson step (which is easily obtained by solving the first order Taylor expansion $f(x) = f(x_n) + f'(x_n)(x - x_n)$), that is

$$x_{n+1} = x_n - \frac{f(x_n)}{f'(x_n)}$$

we obtain

$$x_{n+1} = x_n - \frac{2f(x_n)f'(x_n)}{4\left[f'(x_n)\right]^2 - f(x_n)f''(x_n)} \qquad (7)$$

which is known as the Halley' rational formula. We can note that, thanks to the term $f(x_n)f''(x_n)$, there is no inversion problem when $f'(x_n) = 0$ as long as $f(x_n) \neq 0$ and $f''(x_n) \neq 0$.

We now apply exactly the same reasoning for the case where x and $f(x)$ are not scalars but vectors.

B. General case

Let $\mathbf{p}$ and $\mathbf{p}^*$ be the parameters that represent the current and the desired camera poses. The first order Taylor expansion of $\mathbf{s}(\mathbf{p})$ is given by

$$\mathbf{s}^* = \mathbf{s} + \mathbf{J_s}\Delta\mathbf{p}$$

where $\Delta\mathbf{p}$ represents the displacement between $\mathbf{p}^*$ and $\mathbf{p}$. We immediately deduce the following control law using the Newton-Raphson method:

$$\mathbf{v}_1 = -\lambda_1 \mathbf{L_s}^+ (\mathbf{s} - \mathbf{s}^*) \tag{8}$$

where $\mathbf{J_s}$ and $\mathbf{L_s}$ are linked by $\mathbf{L_s} = \mathbf{J_s}\mathbf{P}$ where $\mathbf{P}$ is defined such that $\dot{\mathbf{p}} = \mathbf{P}\mathbf{v}$. Note that control law (8) is nothing but the classical control law C.

Let us now consider the second order Taylor expansion of $\mathbf{s}$. It is given by

$$\mathbf{s}^* = \mathbf{s} + \mathbf{K}_2\,\Delta\mathbf{p} \tag{9}$$

where matrix $\mathbf{K}_2$ is

$$\mathbf{K}_2 = \mathbf{J_s} + \frac{1}{2}\begin{bmatrix} \Delta\mathbf{p}^\top \mathbf{H}_{s_1} \\ \cdots \\ \cdots \\ \cdots \\ \Delta\mathbf{p}^\top \mathbf{H}_{s_k} \end{bmatrix}$$

Solving (9) for $\Delta\mathbf{p}$, we obtain

$$\Delta\mathbf{p} = -\mathbf{K}_2^+ (\mathbf{s} - \mathbf{s}^*)$$

from which we deduce the following control law:

$$\mathbf{v} = -\lambda \mathbf{K_s}^+ (\mathbf{s} - \mathbf{s}^*) \tag{10}$$

where the output (8) of control law C is used to go from $\mathbf{K}_2$ to $\mathbf{K_s}$:

$$\mathbf{K_s} = \mathbf{L_s} - \frac{\lambda_1}{2}\begin{bmatrix} (\mathbf{s} - \mathbf{s}^*)^\top \mathbf{L_s}^{+\top} \mathbf{H}_{s_1} \\ \cdots \\ \cdots \\ \cdots \\ (\mathbf{s} - \mathbf{s}^*)^\top \mathbf{L_s}^{+\top} \mathbf{H}_{s_k} \end{bmatrix}$$

This control law is named K in the following. Let us note that, if $\mathbf{L_s}$ is singular, it does not necessarily imply that $\mathbf{K_s}$ is singular thanks to the Hessian part involved in this control scheme. Furthermore and contrarily to the control law (5) based on the Newton method, when $\mathbf{L_s}$ is singular, the configurations such that

$$(\mathbf{s} - \mathbf{s}^*) \in \mathcal{N}\left(\mathbf{L_s}^\top\right)$$

does not generally correspond to a local minimum. That are for good points of K. Unfortunately, some bad points also exist. First, $\mathbf{K_s}$ may be singular for some configurations where $\mathbf{L_s}$ is not singular. Then, for $\mathbf{s} = \mathbf{s}^*$, $\mathbf{K_s}$ is singular when $\mathbf{L_{s^*}}$ is singular (since $\mathbf{K_s} = \mathbf{L_{s^*}}$ in that case. However, since we never have $\mathbf{s} = \mathbf{s}^*$ in practice, due to unavoidable image noise, we will never have exactly $\mathbf{K_s} = \mathbf{L_{s^*}}$, which makes appealing the use of K when $\mathbf{L_{s^*}}$ is singular. Furthermore, near the singularity, the low conditioning of $\mathbf{L_s}$ in the first part of $\mathbf{K_s}$ is compensated by the high conditioning of $\mathbf{L_s}$ in

its second part. However, we will see in Section V that if the rank of $\mathbf{K_s}$ is indeed improved, it increases the sensitivity of the control scheme to the image noise.

Following the same idea than going from control law C to D, we could think of using:

$$\mathbf{v} = -\lambda \mathbf{K_{s^*}}^+ (\mathbf{s} - \mathbf{s}^*) \tag{11}$$

where $\mathbf{K_{s^*}}$ is given by:

$$\mathbf{K_{s^*}} = \mathbf{L_{s^*}} - \frac{\lambda_1}{2}\begin{bmatrix} (\mathbf{s} - \mathbf{s}^*)^\top \mathbf{L_{s^*}}^{+\top} \mathbf{H}_{s_1} \\ \cdots \\ \cdots \\ \cdots \\ (\mathbf{s} - \mathbf{s}^*)^\top \mathbf{L_{s^*}}^{+\top} \mathbf{H}_{s_k} \end{bmatrix}$$

However, that is definitively not a good idea since this control scheme has exactly the same bad properties of D that all configurations such that

$$(\mathbf{s} - \mathbf{s}^*) \in \mathcal{N}\left(\mathbf{L_{s^*}}^+\right)$$

will lead to a local minima (to check that, just note that in that case $(\mathbf{s} - \mathbf{s}^*)^\top \mathbf{L_{s^*}}^{+\top} = \mathbf{0}$, which implies $\mathbf{K_{s^*}} = \mathbf{L_{s^*}}$).

A last control scheme can be obtained by considering each feature independently in the second part of $\mathbf{K_s}$, that is using

$$\mathbf{v}_i = -\lambda_1 \mathbf{L}_{s_i}^+ (s_i - s_i^*) \tag{12}$$

instead of (8). In that case we obtain

$$\mathbf{v} = -\lambda \mathbf{K}_i^+ (\mathbf{s} - \mathbf{s}^*) \tag{13}$$

where

$$\mathbf{K}_i = \mathbf{L_s} - \frac{\lambda_1}{2}\begin{bmatrix} (s_1 - s_1^*)^\top \mathbf{L}_{s_1}^{+\top} \mathbf{H}_{s_1} \\ \cdots \\ \cdots \\ \cdots \\ (s_k - s_k^*)^\top \mathbf{L}_{s_k}^{+\top} \mathbf{H}_{s_k} \end{bmatrix}$$

This control law will be named Ki in the following. Even if we are currently unable to give any theoretical explanation, we will see in Section V that this control law allows improving the accuracy of the positiong in a singular configuration.

IV. HESSIAN MATRICES OF AN IMAGE POINT

In the experiments presented in the next section, we will compare the behavior of the control schemes presented in this paper in the case of a target composed of three points. The analytical form of the Hessian matrices $\mathbf{H}_x$ and $\mathbf{H}_y$ of the coordinates (x, y) of an image point are thus needed. Let us note that these matrices have already been used in [7], but the analytical form given in that paper contains unfortunately few typos errors.

A. Modeling

We recall that an image point with coordinates (x, y) results from the perspective projection of a 3D point such that $x = X/Z$ and $y = Y/Z$ where (X, Y, Z) are the coordinates of this 3D point expressed in the camera frame. We also recall that the velocity $(\dot{x}, \dot{y})$ of an image point is linked to the camera velocity $\mathbf{v} = (v_x, v_y, v_z, \omega_x, \omega_y, \omega_z)$ through the well known equations:

$$\dot{x} = \mathbf{L}_x \mathbf{v} \ , \ \dot{y} = \mathbf{L}_y \mathbf{v} \tag{14}$$

where the interaction matrices $\mathbf{L}_x$ and $\mathbf{L}_y$ are given by:

$$\mathbf{L}_x = \begin{bmatrix} \frac{-1}{Z} & 0 & \frac{x}{Z} & xy & -(1+x^2) & y \end{bmatrix} \tag{15}$$

$$\mathbf{L}_y = \begin{bmatrix} 0 & \frac{-1}{Z} & \frac{y}{Z} & (1+y^2) & -xy & -x \end{bmatrix} \tag{16}$$

The Hessian matrices $\mathbf{H}_x$ and $\mathbf{H}_y$ can easily be determined by differentiating (14). Indeed, for any feature s, we have:

$$\ddot{s} = \mathbf{L}_s \dot{\mathbf{v}} + \mathbf{v}^\top \mathbf{H}_s \mathbf{v} \tag{17}$$

where $\mathbf{H}_s$ is a symetrix matrix. Using (14), (15) and (16), we obtain:

$$
\begin{aligned}
\ddot{x} = & \ \mathbf{L}_x \dot{\mathbf{v}} + \frac{\dot{Z}}{Z^2} \ v_x + \frac{\dot{x}Z - \dot{Z}x}{Z^2} \ v_z + \\
& (\dot{x}y + x\dot{y}) \ \omega_x - 2x\dot{x} \ \omega_y + \dot{y} \ \omega_z \\
\ddot{y} = & \ \mathbf{L}_y \dot{\mathbf{v}} + \frac{\dot{Z}}{Z^2} \ v_y + \frac{\dot{y}Z - \dot{Z}y}{Z^2} \ v_z \\
& + 2y\dot{y} \ \omega_x - (\dot{x}y + x\dot{y}) \ \omega_y - \dot{x} \ \omega_z
\end{aligned}
$$

By substituting (14) for $\dot{x}$ and $\dot{y}$, and knowing that:

$$\dot{Z} = -v_z - yZ\omega_x + xZ\omega_y$$

we obtain after simple developments:

$$
\begin{aligned}
\ddot{x} = & \ \mathbf{L}_x \dot{\mathbf{v}} - \frac{2}{Z^2} v_x v_z - \frac{2y}{Z} v_x \omega_x + \frac{3x}{Z} v_x \omega_y - \frac{x}{Z} v_y \omega_x - \frac{1}{Z} v_y \omega_z \\
& + \frac{2x}{Z^2} v_z v_z + \frac{4xy}{Z} v_z \omega_x - \frac{(1+4x^2)}{Z} v_z \omega_y + \frac{2y}{Z} v_z \omega_z \\
& + x(1+2y^2) \ \omega_x \omega_x - y(1+4x^2) \ \omega_x \omega_y + (1+2y^2 - x^2) \ \omega_x \omega_z \\
& + 2x(1+x^2) \ \omega_y \omega_y - 3xy \ \omega_y \omega_z - x \ \omega_z \omega_z
\end{aligned}
$$

$$
\begin{aligned}
\ddot{y} = & \ \mathbf{L}_y \dot{\mathbf{v}} + \frac{y}{Z} v_x \omega_y + \frac{1}{Z} v_x \omega_z - \frac{2}{Z^2} v_y v_z - \frac{3y}{Z} v_y \omega_x + \frac{2x}{Z} v_y \omega_y \\
& + \frac{2y}{Z^2} v_z v_z + \frac{1+4y^2}{Z} v_z \omega_x - \frac{4xy}{Z} v_z \omega_y - \frac{2x}{Z} v_z \omega_z \\
& + 2y(1+y^2) \ \omega_x \omega_x - x(1+4y^2) \ \omega_x \omega_y + y(1+2x^2) \ \omega_y \omega_y \\
& + (1+2x^2 - y^2) \ \omega_y \omega_z - y \ \omega_z \omega_z
\end{aligned}
$$

from which we deduce by identification with (17)

$$
\mathbf{H}_x = \begin{bmatrix}
0 & 0 & \frac{-1}{Z^2} & \frac{-y}{Z} & \frac{3x}{2Z} & 0 \\
0 & 0 & 0 & \frac{-x}{2Z} & 0 & \frac{-1}{2Z} \\
\frac{-1}{Z^2} & 0 & \frac{2x}{Z^2} & \frac{2xy}{Z} & \frac{-1-4x^2}{2Z} & \frac{y}{Z} \\
\frac{-y}{Z} & \frac{-x}{2Z} & \frac{2xy}{Z} & x(1+2y^2) & -y(\frac{1}{2}+2x^2) & \frac{1-x^2+2y^2}{2} \\
\frac{3x}{2Z} & 0 & \frac{-1-4x^2}{2Z} & -y(\frac{1}{2}+2x^2) & 2x(1+x^2) & \frac{-3xy}{2} \\
0 & \frac{-1}{2Z} & \frac{y}{Z} & \frac{1-x^2+2y^2}{2} & \frac{-3xy}{2} & -x
\end{bmatrix}
$$

and

$$
\mathbf{H}_y = \begin{bmatrix}
0 & 0 & 0 & 0 & \frac{y}{2Z} & \frac{1}{2Z} \\
0 & 0 & \frac{-1}{Z^2} & \frac{-3y}{2Z} & \frac{x}{Z} & 0 \\
0 & \frac{-1}{Z^2} & \frac{2y}{Z^2} & \frac{1+4y^2}{2Z} & \frac{-2xy}{Z} & \frac{-x}{Z} \\
0 & \frac{-3y}{2Z} & \frac{1+4y^2}{2Z} & 2y(1+y^2) & -x(\frac{1}{2}+2y^2) & \frac{-3xy}{2} \\
\frac{y}{2Z} & \frac{x}{Z} & \frac{-2xy}{Z} & -x(\frac{1}{2}+2y^2) & y(1+2x^2) & \frac{1-y^2+2x^2}{2} \\
\frac{1}{2Z} & 0 & \frac{-x}{Z} & \frac{-3xy}{2} & \frac{1-y^2+2x^2}{2} & -y
\end{bmatrix}
$$

B. Positiveness of $\mathbf{H}_x$ and $\mathbf{H}_y$

Using the determinant test to study the positiveness of the Hessian matrices $\mathbf{H}_x$ and $\mathbf{H}_y$, we found that the determinants of the leading principal minor vectors of $\mathbf{H}_x$ and $\mathbf{H}_y$ are $\mathbf{M}_x = (0, 0, 0, \frac{x^2}{4Z^6}, \frac{x^3(1+x^2)}{Z^6}, 0)$ and $\mathbf{M}_y = (0, 0, 0, 0, \frac{y^3(1+y^2)}{Z^6}, 0)$ respectively, where $\mathbf{M}_s[i] = |\mathbf{H}_s[1..i, 1..i]|$. This means that the necessary and sufficient condition for both $\mathbf{H}_x$ and $\mathbf{H}_y$ to be positive semi-definite is that x and y are positive, which is of course not always achieved. This may explain the fact that Newton and Halley's methods based on image point coordinates have a small convergence domain.

V. EXPERIMENTAL RESULTS

The experimental results presented in this section have been obtained on a 6 dof eye-in-hand system (see Figure 1). All the control schemes have been easily implemented thanks to the open source ViSP library [10].

Fig. 1. Experimental system

The task consists of positioning the camera with respect to a target composed of three points (in practice, three white dots on a black background to avoid any image processing problem) using the Cartesian coordinates of the perspective projection of these points in the image. The three points form a rectangle isosceles triangle whose side lengths are equal to 0.06 m, 0.06 m and $0.06 \times \sqrt{2}$ m. The interaction matrix is thus of dimension 6×6 and of full rank 6 but for the singularities exhibited in [11] in which case it is of rank 5. The singularities occur when the optical center of the camera belongs to the surface of the right circular cylinder whose basis is defined by the circle to which the three points belong. From this general result, it is easy to see that if one of the three points appears at the principal point in the image (which corresponds to the image of the optical axis), then the interaction matrix is singular.

The desired pose between the camera and the triangle has thus been chosen such that they are parallel (at a distance of 0.5 m) and one point appears at the principal point (see Figure 2). The initial pose has been chosen very near from the

desired one, that is $\mathbf{p_i} = (0.0022, 0.001, 0.501, 0.8, 0.4, 0.6)$ where the first three components represent the translation expressed in meter, and the last three ones represent the rotation expressed in degree. We are indeed interested in the behavior near the singularity.

Let us finally note that the depth of the points, which appears in the translational term of the interaction matrix and in the Hessian matrix, are estimated at each iteration of the control scheme using a classical pose estimation method. Let us also note that the gain λ_1 involved in K and Ki has been set to 1, and the gain λ involved in all the control schemes has been set to 0.5. This value has voluntarily been chosen very small to show the effects of the singularity and to avoid any unstability due to a too high value of λ. The very large number of iterations in each experiment is thus not significant. As for the singular value decomposition used to compute the pseudo-inverses involved in the different control schemes, the condition number threshold has been set to 0.0001. We recall that the condition number is the ratio between the minimal and the maximal singular values of a matrix, and the threshold is used to compute its rank and to consider if a singular value is zero or not. This relatively high value has been chosen to not damage the robot by forbidding high values in the outputs of the control scheme.

The results obtained for control laws D, C, M, K and Ki are given on Figure 2.a, 2.b, 2.c, 2.d and 2.e respectively. As expected, control law D is always of rank 5. It is thus not surprising that it reaches a local minimum. Contral law C is of rank 6 at the beginning of the servo, which allows the system to near the desired position. It is then of rank 5 due to the high condition number threshold, but for some iterations where it becomes again of rank 6, due to image noise, producing high robot velocities at these iterations. Control law M has not a very satisfactory behavior: even if it is of rank 6 at the beginning of the servo, it fails, as D, in a local minimum. As for K, it is almost always of rank 6, as expected, but it reaches also a local minimum and is quite unstable due to the fact that it is of rank 6. Finally, control law Ki provides with the best behavior, similar to the one of C, but with a better positioning accuracy and less noise.

VI. CONCLUSIONS AND FUTURE WORK

In this paper, we have been interested by the difficult problem of reaching a visual singular configuration. Without any surprise, all classical control schemes have been shown to be unsatisfactory. Control schemes based on second order minimization Halley's method have been proposed to try to improve the behavior of the system near the desired singular position. The experimental results obtained have shown that it is possible to improve the accuracy of the positioning using one of these control schemes. It would be interesting to see if it also the case for other singular configurations, such as the case of the centered circle for instance. It would also be interesting to see if any improvement can be obtained by combining Halley's method with the damped-least-squares method.

REFERENCES

[1] F. Chaumette, P. Rives, and B. Espiau, "Classification and realization of the different vision-based tasks," in *Visual Servoing* (K. Hashimoto, ed.), vol. 7 of *Robotics and Automated Systems*, pp. 199–228, World Scientific, 1993.

[2] F. Chaumette, "Potential problems of stability and convergence in image-based and position-based visual servoing", *The Conference of Vision and Control. LNCIS 237*, pp 66-78, 1998.

[3] F. Chaumette, S. Hutchinson, "Visual servo control Part I: basic approaches", *IEEE Robotics and Automation Magazine*, 13(4):82-90, Dec. 2006.

[4] S. Chiaverini, "Singularity-robust task-priority redundancy resolution for real-time kinematic control of robot manipulators", IEEE Trans. on Robotics and Automation, 13(3):398-410, June 1997.

[5] O. Egeland, M. Ebdrup, S. Chiaverini, "Sensory control in singular configurations- application to visual servoing", *IEEE Int. Workshop on Intelligent Motion Control*, pp. 401-405, Istanbul, Turkey, Aug. 1990.

[6] M. Fruchard, P. Morin, C. Samson, "A fremawork for the control of nonholonomic mobile manipulators", *Int. Journal of Robotics Research*, 25(8), Aug 2006.

[7] J.-T. Lapresté, Y. Mezouar, "A Hessian approach to visual servoing", *RSJ/IEEE Int. Conf. on Intelligent Robot and Systems, IROS'04*, vol. 1, pp. 998-1003, Sendai, Japan, Sep. 2004.

[8] E. Malis, "Improving vision-based control using efficient second-order minimization techniques", *ICRA'04*, pp 1843-1848, New Orleans, Apr. 2004.

[9] E. Marchand, F. Chaumette, A. Rizzo, "Using the task function approach to avoid robot joint limits and kinematic singularities in visual servoing", *IEEE/RSJ Int. Conf. on Intelligent Robots and Systems, IROS'96*, vol. 3, pp. 1083-1090, Osaka, Japan, 1996.

[10] E. Marchand, F. Spindler, F. Chaumette, "ViSP for visual servoing: a generic software platform with a wide class of robot control skills", *IEEE Robotics and Automation Magazine*, 12(4):40-52, Dec. 2005,

[11] H. Michel and P. Rives, "Singularities in the determination of the situation of a robot effector from the perspective view of three points," Tech. Rep. 1850, INRIA Research Report, Feb. 1993.

[12] Y. Nakamura and H. Hanafusa, "Inverse kinematics solutions with singularity robustness for robot manipulator control" Trans. ASME Journal of Dynamic System, Measures and Control, 108:163171, Sep. 1986.

[13] B. Nelson, P. Khosla, "Strategies for increasing the tracking region of an eye-in-hand system by singularity and joint limits avoidance", *Int. Journal of Robotics Research*, 14(3):255-269, 1995.

[14] J. Ortega, W. Rheinboldt, *Iterative Solution of Nonlinear Equations in Several Variables*. SIAM. Philadelphia, 2000.

[15] C. Samson, M. Le Borgne, B. Espiau, *Robot Control: The Task Function Approach*, Clarendon Press, Oxford, 1991.

[16] C. Wampler, "Manipulator inverse kinematics solutions based on vector formulations and damped least squares method", *IEEE Trans. on Systems, Mans and Cybernetics*, 16(1):93-101, Jan. 1986.
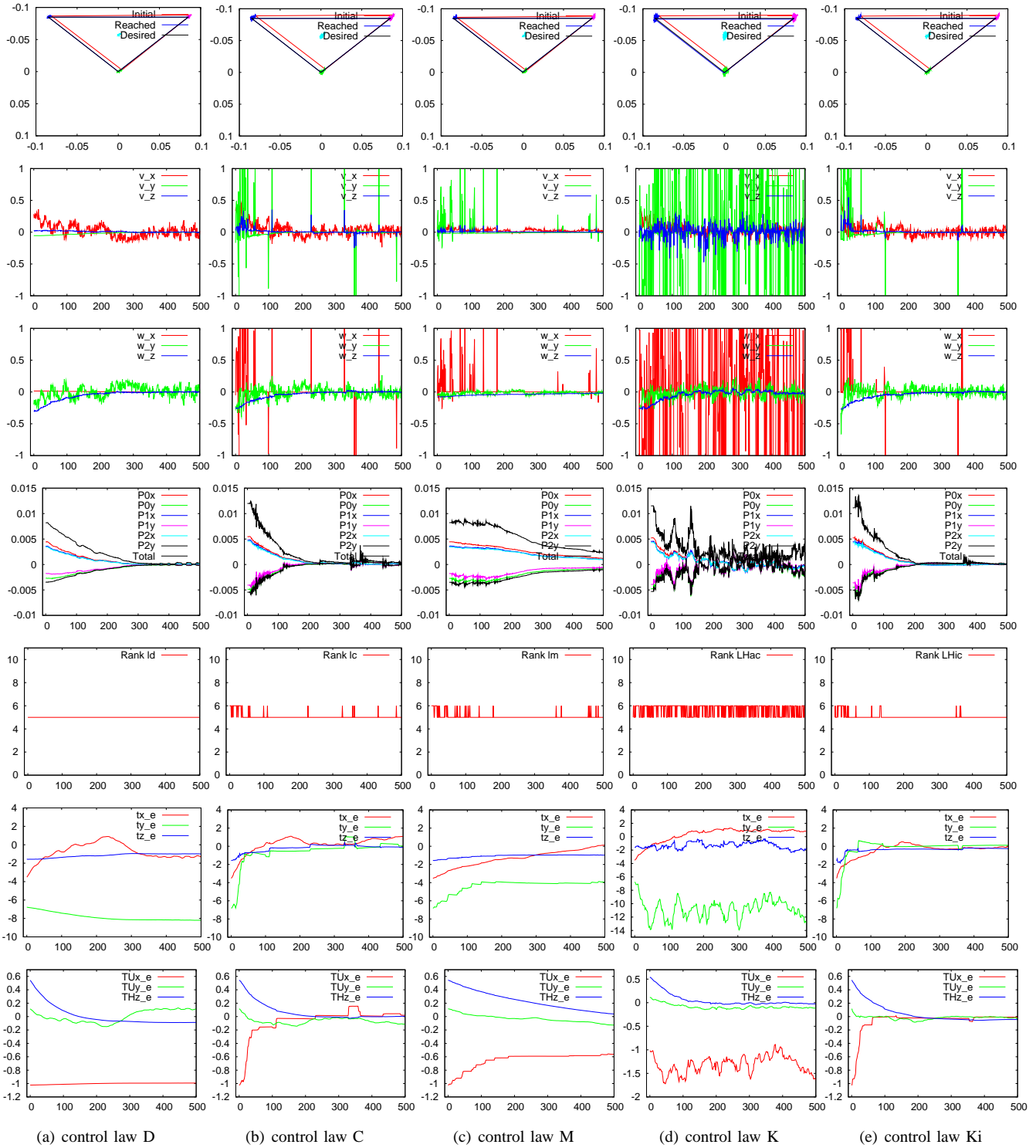
Fig. 2. Experimental results. First line: initial and desired images; second line: translational components of the control law (cm/s); third line: rotational components (dg/s); fourth line: visual features errors; fifth line: rank of the control matrix; sixth line: translational error (in mm); last line: rotational error (in dg)